Crack propagation of a thin hard coating under cyclic loading: irreversible cohesive zone model

J. Feng[1*], Y. Qin[2], T.W. Liskiewicz[1], B.D. Beake[3], S. Wang[4]

[1]Department of Engineering, Faculty of Science and Engineering, Manchester Metropolitan University, Manchester, M1 5GD, UK

[2]Department of Design, Manufacturing and Engineering Management, University of Strathclyde, Glasgow, G1 1XJ, UK

[3]Micro Materials Ltd, Willow House, Yale Business Village, Ellice Way, Wrexham, LL13 7YL, UK

[4] Engineering Services Analysis Limited, Altringham, Cheshire, WA14 5GL, UK

*Corresponding author: Dr. Jiling Feng, j.feng@mmu.ac.uk; Tel: (+44) 161 247 1650.

Abstract:

The numerical study of the fatigue behaviour of steel and light alloy substrates when coated with thin hard coatings is limited. This paper aims to investigate the fatigue failure mechanism of the coating system by observing the initiation and propagation of cracks within the coating under the cyclic loading. The model coating system is composed of three layers: the TiN coating, a case-hardened diffusion zone and the H11 steel substrate. The cohesive elements were arranged evenly in the horizontal direction and vertically through the thickness of the coating layer in order to observe the crack initiation and propagation. The model coating system was indented by a spherical indenter of 300 μm radius. Both the coating and the substrate were characterised as being homogenous, with elastic properties followed by linearly-hardening plastic behaviour. The irreversible cohesive zone model, allowing for the local degradation of the material properties to be incorporated into the model, was employed to simulate the crack initiation and propagation under cyclic loading. It was observed that the crack was initiated at the edge of the contact area between the indenter and coated surface at early stage of loading

cycles, then progressed rapidly through the thickness of the coating layer. The deepest crack was found at 1.4 μm below the top surface. The study has demonstrated that the irreversible cohesive zone model can be used to track the evolution of crack propagation with cyclic loading, therefore has the capability to predict the loading bearing capacity of the coating system under contact fatigue loading conditions.

Keywords: irreversible cohesive zone model, damage variable, cyclic loading

Research Highlights

- Local changes of material properties are incorporated in the model.
- Damage variable captures progressive degradation of material.
- Crack propagation dynamics are correlated with increasing loading cycles.
- Evolution of deteriorating material properties is tracked within the contact area.
- The model predicts surface loading bearing capacity under fatigue conditions.

1. Introduction

Hard physical vapour deposited (PVD) coatings are being increasingly used on relatively softer substrates to improve their performance in applications with harsh working environments such as in machining tools, dies and gears. In the aerospace and automobile industries there is also an increasing trend to protecting parts with high performance coatings that display improved tribological and anti-corrosion properties [1]. In cutting tools and dies for moulding, coatings are usually exposed to complex loading conditions and cracking or delaminating may occur at the interfaces between layers. Coating mechanical properties have been investigated by theoretical, numerical and experimental studies of the indentation test [2-5].

The influence of the coatings on the fatigue and the corrosion fatigue behaviour of mechanical components has been mainly investigated through experimental testing. For example, Puchi-Cabrera and co-workers investigated the rotating bending fatigue behavior of 316L stainless steel coated with TiN coating. In comparison with uncoated steel, they found that the fatigue limit of the TiN coated material at 5×10^6 load cycles was increased by 22% [6]. In addition, significant increase of fatigue strength was observed in both the PVD CrN-coated stainless steel and H11 tool steel, by comparing with uncoated samples [7-8]. However, a significant reduction of fatigue life and fatigue limit was found for the Cr coating on quenched and tempered 4140 structure steel [9]. More recently, Beake, Liskiewicz and co-workers studied the role of coating mechanical properties on the fatigue resistance of two commercial hard carbon coatings on hardened tool steel through micro-impact testing [10]. They found that the harder carbon coating studied, with higher sp^3/sp^2 bonded C (Dymon-iC), was significantly less durable under fatigue loading than the softer carbon coating (Graphit-iC). Several studies reported that micro crack/wear damage occurred during the first few loading cycles [11-12].

Numerical analysis of fatigue behaviour of both steel and light alloy when coated with thin hard coating has been little studied so far due to (i) the limitation of the computation capability in term of the temporal evolution and mesh size, (ii) challenges of the complicated contact boundary conditions and (iii) evolution of the material properties with history of loading. To date, only a few studies have investigated fatigue damage for coated gears [13-14].

Indentation is used widely to quantify mechanical properties of coatings or thin films. Cracking of coatings in the coated tool steel sample is one of the common failure-forms observed during the indentation tests. Under the pressure of an indenter, cracks may initiate from the coating surface or from the coating side of the interface, and they may grow into through-thickness cracks [15-17]. The delamination may occur at the interface due to dissimilarity of the material properties between the coating and substrate [18-19].

Cohesive-zone modelling has been proved to be an efficient approach to simulate fracture of multi-layered coatings and delamination of interfaces under monotonic loading [20, 21]. With the concept of cohesive law, cracks within coatings and delamination between coating/substrate interface can be viewed as a phenomenon where gradual material separation behaviour occurs across the two virtual adjacent surfaces (cohesive zone). This separation follows a softening constitutive equation, which represents the progressive degradation of material strength through a relationship between cohesive traction and material separation across crack surfaces. To date, the cohesive constitutive equation described above has only been employed to investigate the crack formation and propagation under monotonic loading. Under cyclic loading conditions, the response of the model coating system to the loading history is expected to be determined by the damage evolution equation [22-23]. Nguyen et al. revealed that crack subjected to constant-amplitude cyclic loading, and obeying a cohesive law with elastic unloading, tends to shakedown, i.e., after a small number of cycles, material, including the cohesive zone, undergoes elastic deformation leading to the crack arrest [22].

Nguyen developed the irreversible cohesive constitutive equation, by incorporating the damage variable, D, which allows for the energy dissipation resulted from frictional interaction of asperities along the cohesive surfaces and crystallographic slip to be taken into account. This model, considering the unloading-reloading hysteresis, may avoid the possibility of shakedown and attendant spurious crack arrest [23]. Based on damage mechanics theory, Roe and Siegmund developed the cyclic cohesive zone model by incorporating the damage evolution equation into a monotonic cohesive zone model, enabling the degradation of material properties with cyclic loading to be investigated [24]. To date, the fatigue behaviour of the coated surface system investigated by means of cohesive zone model has not been reported.

To enhance the substrate performance and provide better load support to the coating layers, a tool may be heat treated prior to coating application. Plasma-nitriding, for example, is often used to treat cutting- or forming-tools [25]. As a result of this, a hardened layer is produced, called a "hardened case", forming a typical “three-layer” coating-substrate system. Computational modelling of coating damage has mainly focused on non-case-hardened substrates [13]. In this current study, the effect of plastic deformation of the hardened case on the performance of coating layer will be investigated. The irreversible cohesive zone model, which incorporates energy dissipation during unloading-reloading process, will be used to investigate the initiation and propagation of cracks under cyclic loading. The following Methods section describes the details of the cohesive law under monotonic and cyclic loading.

2. Methods

2.1 Cohesive law

2.1.1 The cohesive zone model with non-mechanism dissipation

Fundamentally, the cohesive traction can be derived from an interfacial potential, or the free energy density potential [23], φ

$$T = \frac{\partial \varphi}{\partial \delta} \quad (1)$$

where, T and δ represent the cohesive traction and displacement/separation across the two adjacent virtual surfaces, respectively. A variety of potential forms, including exponential, polynomial and linear forms, have been adopted in previous studies. Fig. 1(a) shows a bilinear traction-separation model that assumes an initially linear-elastic behaviour, followed by the initiation and evolution of damage. The elastic behaviour is determined by the linear relationship between the nominal stresses and the nominal strains across interface. The default value of the original constitutive thickness is set to 1.0 if the traction-separation response is specified, which ensures that the nominal strain is equal to the separation. The area integrated over the traction separation curve provides a measure of the work of separation to create the two surfaces of a developing crack, therefore this value can be considered to be equivalent to the critical energy-release rate, φ. The bilinear traction-separation law can be written as follows:

$$\varphi = \int_0^{\delta_c} T(\delta) \cdot d\delta = \frac{1}{2} T_{max}\, \delta_c \quad (2)$$

where T and δ represent the traction and the separation respectively, T_{max} is the maximum traction and δ_c is the characteristic cohesive-zone length to which the separation reaches upon new crack surface generation. A crack in the coating layer may be initiated when separation reaches a critical value of δ_0, at which point the traction achieves its maximum value, T_{max}. The response of a cohesive element is governed by either the area under the curve of the traction versus displacement, φ, or the characteristic cohesive-zone length, δ_c, once the onset of a crack is encountered.

Due to the original constitutive thickness being specified as 1.0, which implies that the nominal strain is equal to the separation, and the interfacial elastic stiffness, K, representing the ratio of traction to separation, can be taken as same as the Elastic Modulus of the coating, 300 GPa [Table 1]. A nominal-strain criterion, δ_0 , which is used to assess the initiation of cracking, was set as δ_0 = 1%.

2.1.2 Cohesive Zone Model with unloading-reloading hysteresis

Under fatigue loading, material properties of the coating are expected to deteriorate with increasing numbers of cycles, where the prevailing cohesive strength is related to the loading history. The damage variable, D, introduced by Roe and Siegmund [24], allows for the degradation of mechanical and material properties to be accommodated in the cohesive constitutive equation. The modified constitutive equation incorporating the damage variable, D, is given by equation (3) below, where K represents the cohesive zone stiffness. The irreversible cohesive zone model, which allows for the degradation of the material properties with the loading history, is illustrated in Fig. 1(b).

$$T = K\,(1 - D)\delta \tag{3}$$

2.1.3 Determination of the damage variable

The damage variable, D, was defined as the effective surface density of microdefects in the interface [26]. The current value of damage variable is given by the ratio of the damaged cross-sectional area to initial cross-sectional area. Under the conditions of cyclic loading, the damage variable, D_c, is introduced to modify the cohesive constitutive equations, which can capture the failure of the cohesive zone at subcritical loading. The damage variable, D_c, encompasses the well-known characteristics of typical damage evolution laws [26]:

(1) The damage should not occur until the accumulated or current separation is greater than a critical distance, δ_0;

(2) The increment of damage is dependent on the increment of separation;

(3) The endurance limit is based on the traction level, under which the cyclic loading can proceed without causing failure.

The current value of the damage variable, D_c, is calculated by integration of the derivative of damage variable under cyclic loading, $\dot{D}_c$:

$$D_c = \int \dot{D}_c dt \tag{4}$$

where $$\dot{D}_c = \frac{|\dot{\delta}|}{\delta_c}\left[\frac{t}{T_{\max}} - C_f\right]H(\delta - \delta_0) \tag{5}$$

where, $\dot{\delta}$ is the derivative of the separation, t is the traction along the thickness direction, and $C_f = \frac{\sigma_f}{T_{\max}}$ is coefficient ensuring the endurance limit for damage accumulation, where σ_f is the cohesive zone endurance limit.

In this study, the majority of the parameters of cohesive zone model for cyclic loading are the same as those used in the cohesive zone model for monotonic loading [27] such as critical distance, δ_0, is taken as 1% and the maximum traction, T_{max}, is 0.3 GPa which is calculated by critical distance multiplying by the stiffness of the coating, K, $T_{max} = \delta_0 \times K$. The characteristic cohesive-zone length was taken as 5% [27]. Endurance limit for damage accumulation, $C_f = 0.25$ as suggested by Roy and Siegmund [24].

The evolution of damage needs to encompass both monotonic and cyclic loading cases. In the FE package (Abaqus, 2019) that has been used for the modelling, the current value of the

damage variable under the monotonic loading, D_m, is calculated from the separation of opposite virtual surface. The formula for calculating D_m is

$$D_m = \frac{\delta_c}{\delta}\frac{(\delta - \delta_0)}{(\delta_c - \delta_0)} \qquad (0 \le D_m \le 1) \tag{6}$$

where δ is the separation of two virtual faces of cohesive element, δ_0 the criterion separation of initiation of the crack and δ_c is the critical separation indicating the cohesive element is fully damaged. With two different damage mechanisms defined, the greater of two values will always be stored as the current damage:

$$D = \max(D_{c,} D_m) \tag{7}$$

The cohesive properties described above were written using Intel Fortran (Intel Fortran, 2019) by applying an in-house code, which allows the degradation of material properties to be incorporated into FE models by using Abaqus User Material (UMAT) Subroutine.

2.2 Numerical Model

Fig.2 represents the structure of a cylindrical multi-layered system indented by a spherical indenter [27]. In term of the geometrical features and loading conditions, the problem can be assumed as an axi-symmetric one, therefore, only one half of this model is needed to simulate three dimensional (3D) problem. The model coating system is composed of three layers: the TiN coating, the diffusion zone or hardened case, and the H11 steel substrate. The model system was indented by a spherical indenter with 300 μm radius. Both the coating and the substrate were characterised as being homogenous, with elastic properties followed by linearly-hardening plastic behaviour. The material properties of top layer of the substrate (the hardened

case or diffusion zone) were modified to enhance the load-bearing capacity of the coating/substrate system, to simulate the effect of plasma nitriding. The cross-sectional hardness of the hardened layer was converted into the corresponding yield strength using the Tabor factor of 3 [27]. The mathematical function of yield strength (σ_y) versus the depth of the hardened case in the form of polynomial function was obtained by the best-curve fitting technique as shown in Eq (8)

$$Y = \sum_0^N C_n X^n \quad (8)$$

where, Y is yield strength, X is the depth of the hardened case, C_n coefficient, n the index of power and N indicates the items. In this study, sixth power of polynomial function, where C_0=3354, C_1=52.8, C_2=-3, C_3=0.07, C_4=− 0.0008, C_5=4 × 10^{-6}, C_6=−7 × 10^{-9}, was implemented into FE model as field variables to represent the variation of the yield strength along the depth of hardened case [27]. All of the material properties were obtained through experimental testing [27]. The configuration of the coating system model and its material properties are summarised in Table 1.

To observe how the crack was initiated and developed in the coating under cyclic loading, the central section of the coating layer was divided into a series of sub-blocks between each pair of which a cohesive-zone was assumed. To simplify the modelling procedure, cohesive elements were arranged evenly in the horizontal direction and vertically through the thickness of the coating layer (Fig.2). The interval between cohesive elements was determined by dividing the width of the central coating layer by the number of the cohesive element columns to be deployed. The cohesive element thickness was 0.01 μm and the interval of the cohesive zone depended on the density of cohesive zone and the width of model. The model is a parameterised model, edited with Abaqus keywords function, therefore, the meshing scheme is controlled by the parameters concerning the density of the elements and the dimensions of

the model. The element size of the central coating in *x*-direction, for example, can be prescribed by dividing the width of the central coating by the number of element in the same direction in this part [27]. At the same time, the coordinates and the number of corner nodes can also be determined by these parameters.

A contact pair with a small amount of sliding (friction coefficient = 0.05) in the tangential direction was defined for the contact between indenter and the upper coating layer. As shown in Fig. 2, fixed-displacement constraints were applied along the bottom and the right side of the model. A cyclic movement of indenter at a given displacement amplitude of 2 μm was specified for the reference point of indenter, which generated 273 loading cycles with the amplitude at approximately 12 N. The first 5 cycles of loading-unloading are shown in Fig.3.

Table 1. Material properties of coating and substrate studied [27]

Layers	Properties					Dimensions	
	Elastic Modulus (GPa)	Poisson's Ratio, υ	Yield Strength, σ_y (GPa)	Tensile Strength, σ_c (GPa)	Elongation	Thickness (μm)	Width (μm)
Coating (TiN)	300	0.3	4.2	4.4	0.273	2	-
Hardened layer	210	0.3	Function (Eq (8))	-	-	180	-
Substrate (H11 steel)	210	0.3	1.6	1.9	0.09		-

3. Results

3.1 The loading-unloading pattern

The reaction force from the indenter reached a maximum of 12 N when the indenter reached an indentation depth of 2 μm. Increasing contact pressure during loading resulted in sink-in

around the contact with permanent deformation occurring in the substrate. Fig.3 shows that the reaction force was zero when the indenter was displaced by approximately 0.9 μm during the unloading-reloading process. The two vertical lines indicate the range of zero loading force due to the separation of the indenter and coated surface.

The correlation of the loading force and displacement of indenter for all the loading cycles is shown in Fig.4a. In the first cycle the loading and unloading curves are clearly separated (Fig.4b), while in the following cycles the loading path is nearly identical with unloading path. The large hysteresis area formed in the first cycle indicated that the energy dissipation due to the plastic deformation of substrate is mainly occurring in the first cycle. The relationship of the loading force and displacement of indenter for the 2^{nd}, 10^{th} and 23^{rd} cycle, shown in Fig.4c, indicated clearly that the stiffness for the multi-layered surface system during loading is not degraded from the 2^{nd} loading cycle.

3.2 Initiation and development of plastic deformation in the substrate

3.2.1 Plastic deformation during the first cycle

Fig.5 shows the plastic initiation and development during the first loading cycle. As the indenter penetrated to the depth of 0.2 μm, plastic deformation occurred at the centre point of the hardened case immediately underneath the coating layer (Fig.5a). With the increasing depth of the indenter, the reaction force of the indenter and contact area between the indenter and surface of the coating increased. This resulted in a rapidly enlarged area of the plastic deformation in both longitudinally and radial directions (Fig.5b & c). The maximum plastic deformation increased by approximately 20 times when the indenter moved from 0.2 μm to the deepest point of penetration at 2 μm (Fig.5c). There was no further plastic deformation during the unloading process (Fig.5d).

3.2.2 Plastic deformation developing through further unloading-reloading cycles

Plastic deformation mainly occurred during the first cycle, with its development over the rest of the loading cycles being barely visible. The plastic deformation that occurred at the 1st, 2nd, 63rd, 103rd, 203rd and 273rd cycles is shown in Fig.6 (a-e), respectively. The maximum plastic deformation slightly increased over the cycles. For example, the equivalent plastic strain, defined as PEEQ in Abaqus, was 0.0327 at 1st cycle and 0.0395 at 273rd cycle, respectively. The region of the PEEQ in the hardened case remained unchanged. It is noticed that the plastic deformation was initiated in the coating layer at the 63rd cycle with its region gradually enlarged with the increase of the numbers of cycles (highlighted with circles in Fig.6 c,d,e,f).

3.3 Development of the damage variable with loading cycles

The coating properties degraded with increasing loading cycles, ultimately resulting in the fatigue damage of the coating. The degradation of the material properties were simulated using the irreversible cohesive law described in the section 2. Fig. 7 shows the damage variable accumulation over the cycles at the different locations through the thickness of the coating layer. In the top surface of the coating, damage initiated in the first cycle and developed rapidly over the cycles, reaching the maximum value at the 6th cycle and resulting in the initiation of the crack at the surface of coating. Damage of coating material properties developed longitudinally into the depth of coating along the direction of the thickness with the increase number of the loading cycles. At the depth of 0.5 μm and 1 μm under the coating surface, damage reached the critical value at 9th and 13th cycle, respectively. In this study, the deepest crack observed was at a depth of 1.4 μm below the surface. At penetration depths >1.4 μm, the damage variable developed with cycling loading but did not reach the critical value to induce

cracking. For example, at 1.6 μm the damage initiated at 23rd cycle and increased to 0.8 at about 60 cycles, remaining at this level until the end of the loading cycles.

3.4 Crack initiation and propagation

3.4.1 Crack propagation under cyclic loading

The crack initiation and propagation over the loading cycles are shown in Fig.8. Fig.8a shows the maximum principal stress (MPS) distribution in the first loading cycle when the indenter reached the maximum value of displacement, 2 μm. The MPS occurs at the edge of contact area of the indenter. Negative values (blue area) of MPS occur at the central area of the hardened case, indicating compressive stress occurring in this area due to the contact pressure applied by the indenter. Fig.8b shows the MPS distribution during unloading process when indenter moved backward to 0.9 μm of the displacement, at which point the indenter was separated from the coated surface. The MPS is lower due to the elastic deformation recovered when the contact pressure of indenter is released. However, it is worth noting that the high value of the residual tensile stress still remained in the edge of contact region of indenter and coating. With increasing number of loading cycles, the material properties degraded with evolution of the damage variable. This eventually resulted in the virtual surface of the cohesive element separation, initiating the occurrence of the crack (Fig.6c). The crack propagated into the depth along the thickness of the coating until the deepest crack reached 1.4 μm.

3.4.2 Crack behaviour during the loading and unloading process

The first crack initiated during the 6th cycle and propagated to the depth of 1.4 μm through the coating thickness. The crack behaved differently during the loading and unloading process in

the following cycles. Fig.9 shows the crack behaviour at the last cycle. It can be seen that the crack gap became smaller during the loading process when the indenter moves downward (left side in Fig.9). The crack is fully closed as the indenter reached the maximum displacement (2 μm). During the unloading process, the contact pressure from the indenter is reduced, which released the compressive stress, then the crack opened again. The crack is fully opened as the indenter is completely separated from the coating surface.

4. Discussion

The fatigue and corrosion behaviour of mechanical components coated with thin hard coatings has attracted a significant interest in the field of machining tools and the other industries such as aerospace and automotive. The influence of the PVD thin hard coatings on the fatigue performance of coated components has been mainly investigated through experimental testing [28, 29]. Most of the numerical modelling studies for the mechanical and damage performance of coated components have mainly focused on the coating characterization [30], rather than the fatigue crack formation and propagation. The most popular approach to assess fatigue fracture cracking is the Paris Law [31]. In general, however, this approach can be viewed as a phenomenological model, i.e. a fitting scheme for experimental data [32]. Theoretical and numerical modelling for crack propagation and fatigue life of coated components is limited, though the subsurface crack initiation and propagation in a very high cycle fatigue regime have been studied [33]. Xu also employed the cyclic cohesive zone model, combined with extended finite element method, to simulate fatigue crack propagation under mixed loading conditions [34]. To the best of the authors' knowledge, numerical study of crack formation and propagation for the coating under contact cyclic loading has not been widely reported.

4.1 Evaluation of the fatigue damage of the coated system using the irreversible cohesive law

Roe and Siegmund [24], taking the monotonic cohesive zone model as a starting point, developed a cyclic cohesive zone model by introducing the damage evolution equation. This equation is based on a well-known continuum damage theory, proposed by Lemaitre and Chaboche in 1990 [35]. The key points of continuum damage law proposed by these authors can be summarized as: (1) damage initiates once the deformation measure meets a threshold criterion; (2) the damage rate is proportion to the deformation measured at the current load level; (3) the damage only accumulates beyond an endurance limit. The damage variable, D_c, described in Eq (4) and (5), meets all of the criteria of evolution damage law above.

The cyclic irreversible cohesive zone model described above, is employed in this study to simulate the crack formation and propagation of the thin hard coating under cycling loading. The cyclic irreversible cohesive constitutive equation takes into account the energy dissipation resulting from frictional interaction of asperities along the cohesive surfaces and crystallographic slip, therefore, preventing from the possibility of shakedown and attendant spurious crack arrest [23]. By introducing the evolution of the damage variable, the irreversible cohesive law described in Fig.1 (b) allows for the localized mechanical and material properties dependent on the loading history to be incorporated into the FE model. The initiation and evolution of the damage related to the loading history at the various depths were clearly shown in Fig.7. At the edge of indented area, the damage was induced during the first cycle, and then progressed rapidly to the critical value with the increasing number of loading cycles, eventually initiating circumferential crack in the surface of coating. The circumferential cracks observed in the numerical study were comparable to the experimental observation in term of diameter of

circumferential cracks under the same loading conditions [27]. This study has demonstrated that the evolution of the local material damage to the contact fatigue loading history can be quantitatively evaluated. The cohesive element model, embedded within coated layer, allows for the crack initiation and propagation via the loading history to be observed. The results of this study have shown that the load bearing capacity of the coated system under the contact fatigue loading can be predicted using the irreversible cohesive law approach.

4.2 Effect of the plastic deformation on the damage of thin coating

In this study, the plastic deformation mainly occurred in the central part of the hardened case. With increasing penetration of the indenter, this region of plastic deformation expanded rapidly, accompanied by the magnitude of the equivalent plastic deformation increasing dramatically. The energy dissipation, caused by plastic deformation in the hardened case, mainly occurred in the first cycle, which is also reflected by the hysteresis area formed by the reaction force and displacement of indenter (shown in Fig.4). This observation is consistent with the observation of cyclic plastic deformation of the rolling contact under repeatedly contact loading observed by Hwang and co-workers [36]. They found that plastic deformation occurred only at first few cycles and became purely elastic in the subsequent cycles due to the existing residual stresses and material hardening. In our study, the plastic deformation caused the material of hardened case flowing toward the outside of contact region, which resulted in the bending of the coating at the edge of the contact region. Similar to findings from Abdul-Baqi and Gómez-Ovalle [2, 19], the significant increase of tensile stress (shown in Fig. 8a) due to coating bending was observed at the coating surface close to the contact edge. This high value of tensile stress initiated the localized material degradation, and eventually caused the damage of the coating. In the subsequent loading cycles no further plastic deformation developed in the hardened case.

4.3 Prediction of the load bearing capacity under the contact fatigue loading condition

The previous studies demonstrated that the cohesive zone model can predict load bearing capacity of coated systems under the monatomic loading through tracking the initiation and propagation of cracks within the coating [14, 20, 21, 27]. In this study, the irreversible cohesive zone model, allowing for the crack initiation and propagation to be tracked under cyclic loading, has been used to predict the loading bearing capacity under the fatigue loading condition. The model used in this study has been validated by an experimental indentation test under monotonic loading. It was found in both experimental and simulation study that the first crack was initiated at a higher load of 30 N when a 200 um spherical indenter is applied [27]. It was observed in this study at the lower load of 12 N that although damage was initiated during the first cycle, the first crack was observed during the 6^{th} cycle. This difference indicates that the load bearing capacity predicted with the single loading is not sufficient to estimate the loading bearing capacity of the coated product under the fatigue loading condition. The loading conditions in this study (2 μm displacement/12 N) were carefully selected in order to observe the evolution of crack initiation and propagation. With the model used in this study, it was observed that there is no crack occurring if displacement from indenter is less than certain level, e.g 1.8 μm. In contrast, cracking can occur during the early stage of the first loading cycle if the loading from the indenter is too large. With the loading level selected in this study, the crack initiation and propagation under cyclic loading was clearly observed. This study has demonstrated the potential of the irreversible cohesive zone model as a tool to predict the loading bearing capacity of coated systems under contact fatigue loading conditions.

4.4 Experimental evidence for coating fatigue behaviour under cyclic loading conditions

Although the model has not been validated under cyclic conditions, several experimental studies with sharper and blunter probe geometries [10-12, 37-40] have shown that hard PVD coatings can display a level of fatigue behaviour under cyclic loading. In addition to the coating mechanical properties, the type of cracking observed depends on a range of factors including probe geometry, coating thickness, severity of loading and number of cycles. For example, Tarrés and co-workers reported the damage progression behaviour described in this study – a surface crack at the contact periphery gradually growing down from the top surface with increasing cycles – occurred under cyclic loading of a PVD TiN coating on hard metal substrate by a 1.25 mm radius WC-Ni spherical indenter. By evaluating the critical loads for cracking under monotonic and fatigue loading these authors were able to determine a fatigue sensitivity for the coating [39]. The location of the crack at the top surface at the periphery of the contact predicted by the model has also been seen in experimental studies of repetitive micro-scale impact by spherical indenters with smaller end radii (17-20 μm). For example, Beake, Liskiewicz and co-workers used the recently developed micro-impact technique to investigate the micro-scale impact resistance of hard carbon coatings on hardened tool steel [10,12,37] and PVD nitrides on cemented carbide [11,12, 38].

Although the spherical probe geometry used in this study is generally preferred for investigating repetitive indentation/impact damage evolution and fatigue sensitivity [39], fatigue type behaviour has also been observed for sharper probe geometries in a wide range of hard coatings. For example, in some PVD coatings surface radial cracks can develop which grow gradually away from the impact zone with increasing number of cycles and/or load. In cyclic Vickers indentation of hard coatings on tool steels the type of cracking depended on the

H/*E* ratio of the coatings [40]. A quasi-plastic damage mode with radial cracks that grew with number of cycles was typical in lower *H*/*E* coatings.

Bouzakis and co-workers have modelled repetitive nano-impact tests of TiAlN coatings with a much sharper diamond cube corner probe [41-43]. They developed 3D-FEM and 2D axis-symmetric FEM models using the ANSYS LS-DYNA software to simulate the damage progression in repetitive nano-impact tests on PVD Ti,AlN coatings with sharp cube corner (*R* ~0.075 μm end radius) indenters. Its feature of constrained tied nodes failure was used for simulating crack formation and propagation, as the plastic strain develops and exceeds the coating failure strain. The impact-induced stresses were more localised with the much sharper probe geometry in the nano-impact test resulting in differences in the failure behaviour to when blunter spherical probes are used.

Similar to the material properties used in this study, Bouzakis et al also consider the material properties of coating layer as elastic-plastic with the properties of Elastic Modulus, Yield Stress and Rupture Stress, which are equivalent to the properties in our study. One reason for cyclic hardening of the layer was not observed very clearly in this study might be due to the large curvature of the indenter acting on the very thin layer, although Bouzakis and co-workers have reported effective simulation of the damage observed experimentally in tests with a sharper probe without incorporating cyclic hardening in their model. The implementation of the cohesive zone within the coating might have some effect on the simulation results although this method has been previously validated through monotonic loading. In future, we plan to conduct repetitive micro-impact tests to validate the model, and if needed, the model will be further modified in combination with other modelling methods such as X-FEM.

4.5 Model limitations

The finite element model employed in this study was used to investigate the crack formation and propagation within the coating under the monotonic loading. In terms of the loading level when the crack is induced and the location of the circumferential crack, the numerical results are in agreement with the experimental test results under monotonic loading. In this study, this model was further developed by implementation of the cyclic irreversible cohesive law into the coating material, which enables the degradation of the material properties with loading history to be investigated. A full experimental validation of this modified model with the cyclic loading conditions has not been conducted. It has no doubt that further experimental investigation, aiming to validate the modified numerical model, needs to be investigated in future.

The mixed failure mode, including the crack within the coating and interfacial delamination, were recently investigated by Gómez-Ovalle and co-workers [19] by using extended finite element method (X-FEM) and cohesive zone model with monotonic loading. This study specially focused on the coating crack formation and propagation under the cyclic loading, therefore, the cohesive element was not implemented at the interfacial layers. It is expected that there is a stress concentration at the interfacial layer due to the mismatch of the mechanical properties of coating and substrate, so delamination might occur at some stage of loading. The model used in this study might neglect the effect of the delamination on the coating crack initiation and propagation. Accordingly, the further improvement of numerical model is also needed to encompass the effect of the delamination between the coating and substrate on the damage performance of coating system.

As mentioned above, X-FEM combined with the cohesive zone model approach was used to simulate cracking and delamination of the interfacial layer by Gómez-Ovalle [19] under monotonic loading. In our previous study [27] the model developed for the monotonic loading

was validated experimentally as the existence of a cohesive zone might have an effect on the stress distribution. However, due to a very low thickness (0.01 microns) of the cohesive zone layer, its effect on the stress distribution and general stiffness of the system is found to be negligible. This has been confirmed by good agreement between the experiments and numerical modelling observed in the monotonic loading. In this study however, the numerical approach has not been compared with the other methods, such as X-FEM. Notwithstanding these limitations, the results presented in this work suggest the irreversible cohesive zone model has significant potential for improved reliability in prediction of the load bearing capacity of coated components under fatigue loading conditions.

The cohesive elements implemented in Abaqus allow modelling of progressive damage and failure in cohesive layers. Failure mechanism consists of three ingredients: a damage initiation criterion, a damage evolution law (our study uses bilinear traction-separation law), and a choice of element removal (or deletion) upon reaching a completely damaged state (in our study an element is removed when the damage coefficient reaches 0.9). The cohesive zone model available in Abaqus, however, cannot be directly used for cyclic loading conditions since the material properties, such as stiffness, are constant without considering the damage propagation related to the cyclic loading history. In our study, damage accumulation with each loading cycle was considered, and the effect of this damage accumulation on the degradation of the material properties was iterated at each calculation step. Damage was observed on the first cycle but it was not large enough to cause a crack in the coating until the 6th cycle, when a crack initiated at the top surface. In contrast, with the cohesive zone element model in Abaqus (which does not consider degradation of the properties), cyclic loading will lead to infinite life if the crack is not induced in the first cycle.

The loading level in this study was chosen in order to investigate the damage propagation of a single crack with increasing number of loading cycles. It has been established in our

previous study that multiple cracks could be generated under higher monotonic load [27]. In future it is planned to apply the model under a range of higher applied cyclic loads, in order to simulate multiple crack initiation and propagation.

5. Conclusions

In this study, an irreversible cohesive law, that accounts for the effect of the damage caused by monotonic and cyclic loading on the mechanical and material properties of a model coating system, has been used to investigate the crack initiation and propagation under the contact fatigue loading. The damage variable was incorporated into the cohesive zone model, allowing the material deterioration with the increasing of number of loading cycles to be taken into account. The results indicate that damage began during the early stage of loading cycles and propagated rapidly through the coating thickness. The bending stress at the edge of contact area, caused by the plastic deformation of hardened case, plays an important role in crack initiation. Compressive stress, caused by the indentation contact pressure during reloading, forced crack closure. Subsequent unloading released the compressive stress, prompting re-opening of the crack. The irreversible cohesive zone model has been shown to be potentially a more reliable approach to predict the load bearing capacity of coated components under fatigue loading conditions.

Acknowledgements

The research reported in this paper was supported by the EU FP7 project 'Multiscale Modelling for Multilayered Surface Systems (M3-2S)', Grant No. CP-FP213600-2 M3-2S. Beneficial discussion with and support from the project partners are acknowledged.

References

[1] A.M. Merlo, The contribution of surface engineering to the product performance in the automotive industry, Surf. Coat. Technol. 175 (2003) 21-26.

[2] A. Abdul-Baqi, E.Van Der Giessen, Numerical analysis of indentation-induced cracking of brittle coatings on ductile substrates, Int. J. Solids Struct. 39 (2002) 1427-1442.

[3] J. Michler, E. Blank, Analysis of coating fracture and substrate plasticity induced by spherical indentors: diamond and diamond-like carbon layers on steel substrates, Thin Solid Films. 381(2001) 119-134.

[4] S. Nekkanty, R. Shivpuri, M. Walter, J. Castro, A cohesive zone finite element approach to model tensile cracks in thin film coatings, J. Mech. Mater. Struct. 2 (2007) 1231-1247.

[5] D. Yin, X. Peng, Y. Qin, J. Feng, Z. Wang. Quantifying Adhesion Energy of Mechanical Coatings at the Atomistic Scale, Appl. Surf. Sci. 258 (2011) 1451-1455.

[6] E.S. Puchi-Cabrera, F. Matinez, I. Herrera, J.A. Berrios, S. Dixit, D. Bhat, On the fatigue behaviour of an AISI 316L Stainless steel coated with a PVD TiN deposit, Surf. Coat. Technol. 182 (2004) 276-286.

[7] S. Baragetti, G.M. La Vecchia, A. Terranova, Fatigue behaviour and FEM modelling of thin-coated components, Int. J. Fatigue, 25 (2003) 1229-1238.

[8] S. Baragetti, G.M. La Vecchia, A. Terranova, Variables affecting the fatigue resistance of PVD-coated components. Int. J. Fatigue 27 (2005) 1541-1550.

[9] M.J. Ortiz-Mancilla, C. Mariño-Berroterán, J.A. Berríos-Ortiz, G. Mesmacque, E.S. Puchi-Cabrera, Effect of a thin hard chromium coating on fatigue behaviour of 4140 steel, Surf. Eng. 20 (2004) 345-352.

[10] B.D. Beake, T. W. Liskiewicz, A. Bird, X. Shi, Micro-scale impact testing - A new approach to studying fatigue resistance in hard carbon coatings, Tribol. Int. 149 (2020) 105732.

[11] B.D. Beake, L. Isern, J.L. Endrino, G.S. Fox-Rabinovich, Micro-impact testing of AlTiN and TiAlCrN coatings, Wear 418–419 (2019) 102-110.

[12] B.D. Beake, L. Isern, J.L. Endrino, T.W. Liskiewicz, X. Shi, Micro-scale impact resistance of coatings on hardened tool steel and cemented carbide, Mater. Lett. 284 (2021) 129009.

[13] S. Baragetti, F. Tordini, Fatigue resistance of PECVD coated steel alloy, Int. J. Fatigue 29 (2007) 1832-1838.

[14] J. Feng, Y. Qin, H. Dong, Investigation into initiation and propagation of cracks in the coated surfaces of spur gears with submodelling and irreversible cohesive-zone modelling techniques, Manuf. Rev. 3 (2016) 6-6.

[15] J. Hu, Y.K. Chou, R.G. Thompson, Cohesive zone effects on coating failure evaluations of diamond-coated tools, Surf. Coat. Technol. 203 (2008) 730-735.

[16] K. Shu, C. Zhang, P. Hou, D. Zheng, L. Gu, L. Wang, Crack evolution in diamond-like carbon films on steel substrates during nano-indentation, Diamond Relat. Mater. 106 (2020) 107829.

[17] Y. Xiao, W. Shi, L. Jing, Indentation for evaluating cracking and delamination of thin coatings using finite element analysis, Vacuum. 122(2015) 17-30.

[18] J. Chen and S. J. Bull, Indentation fracture and toughness assessment for thin optical coatings on glass, J. Phys. D: Appl. Phys. 40 (2007) 5401–5417.

[19] A.E. Gómez-Ovalle, M. Torres, S.M.A. Jimenez, et al., Experimental-numerical failure analysis of the c-Al0.66Ti0.34N-M2 steel system applying instrumented indentation and extended finite element method, Surf. Coat. Technol. 393 (2020) 125845.

[20] J. Feng, Y. Qin et al. A new technique to investigate the load-bearing capacity of a coating on tool steel by considering the damage in the coating surface, Proc. IMechE B, J. Eng. Manuf. 226 (2012) 1205-1210.

[21] J. Feng & Y. Qin, Prediction of the critical load of a metal-rolling system by considering the damage of the coated surface, Steel Res. Int. Metal forming, Special Edition, 2012.

[22] O. Nguyen, E. Repetto, M. Ortiz, et al., A cohesive model of fatigue crack growth, Int. J. Fract. 110 (2001) 351–369.

[23] X.-P. Xu and A. Needleman, Numerical simulations of fast growth in brittle solids, J. Mech. Phys. Solids 42 (1994) 1397-1434.

[24] K.L. Roe, T. Siegmund, An irreversible cohesive zone model for interface fatigue crack growth simulation, Eng. Fract. Mech. 70 (2003) 209-232.

[25] J Musil, J Vlček, M Růžička, Recent progress in plasma nitriding, Vacuum 59 (2000) 940-951.

[26] J.A. Lemaitre, A course on damage mechanics, Springer-Verlag, 1996.

[27] J. Feng, Y Qin et al. Parameterised modelling approach for multilayered coating system under indentation, Journal of Multiscale Modelling 3 (2011) 1-22.

[28] S. Baragetti, F. Villa, An updated review of the fatigue behavior of components coated with thin hard corrosion-resistant coatings, Open Mater. Sci. 8 (2014) 87-98.

[29] H. Xu, H. Li, J. Hu and S. Wang, A study on contact fatigue performance of nitrided and TiN coated gears, Adv. Mater. Sci. Eng. (2013), 580470.

[30] S. Baragetti, F Tordini, A review of the fatigue behaviour of components coated with thin hard corrosion-resistant coatings, The Open Corrosion J. 4 (2011) 9-17.

[31] P.C. Paris, M.P. Gomez, W.P. Anderson, A rational analytic theory of fatigue. Trend. Eng. 13 (1961) 9-14.

[32] S. Suresh, Fatigue of Materials, second edition, Cambridge University Press, 1998.

[33] K. Shiozawa, Y. Morii, S. Nishino, L. Lu, Subsurface crack initiation and propagation mechanism in high-strength steel in a very high cycle fatigue regime, Int. J. Fatigue 11 (2006) 1521-1532.

[34] Y. Xu, H. Yuan, On damage accumulations in the cyclic cohesive zone model for XFEM analysis of mixed-mode fatigue crack growth, Comput. Mater. Sci. 3 (2009) 579-585.

[35] J. Lamaitre and J.L. Chaboche, Mechanics of Solid Materials, Cambridge University Press, 1990.

[36] Y. Hwang, Cyclic deformation caused by repeated contact loading, Appl. Mech. Mater. 883 (2018) 8-15.

[37] S. J. McMaster, T. W. Liskiewicz, A. Neville, B. D. Beake, Probing fatigue resistance in multi-layer DLC coatings by micro- and nano-impact: Correlation to erosion tests, Surf. Coat. Technol. 402 (2020) 126319.

[38] B. Beake, L Bergdoll, L. Isern, J.L. Endrino, et al. Influence of probe geometry in micro-scale impact testing of nano-multilayered TiAlCrN/NbN coatings deposited on WC-Co. Int. J. Refract. Met. Hard Mater. 95 (2020) 105441.

[39] E. Tarrés, G. Ramírez, Y. Gaillard, et al., Contact fatigue behavior of PVD-coated hard metals, Int. J. Refract. Met. Hard Mater., 27 (2009) 323-331.

[40] A. Sivitski, A. Gregor, M. Saarna, et al., Application of the indentation method for cracking resistance evaluation of hard coatings on tool steels. Estonian J. Eng. 15 (2009) 309-317.

[41] K.-D. Bouzakis, S. Gerardis, G. Skordaris, E. Bouzakis, Nano-impact test on a TiAlN PVD coating and correlation between experimental and FEM results, Surf. Coat. Technol. 206 (2011) 1936–1940.

[42] G. Skordaris, K.-D. Bouzakis, P. Charalampous, A dynamic FEM simulation of the nano-impact test on mono- or multi-layered PVD coatings considering their graded

strength properties determined by experimental–analytical procedures,Surf. Coat. Technol. 265 (2015) 53-61.

[43] G. Skordaris, K. Bouzakis, P. Charalampous, A critical review of FEM models to simulate the nano-impact test on PVD coatings, MATEC Web of Conferences 188, 04017 (2018).

Figure captions

Fig. 1 (a) The bilinear cohesive zone model; (b) traction-separation cohesive zone law under cyclic loading.

Fig. 2 Geometric model of a multi-layered system including the coating, the hardened case and the substrate.

Fig. 3 The first 5 cycles of loading-unloading by the indenter. (a) the reaction force acted on the surface of coating by the indenter with the amplitude approximately at 12 N; (b) cyclic movement with the amplitude of 2 μm specified to reference point of indenter. The two vertical lines indicate the time points between which the indenter is separated from coating surface.

Fig. 4 The correlation of the force and the displacement of the indenter for 273 cycles (a), at the 1^{st} cycle (b) and at the 2^{nd} , 10^{th} and 23^{rd} cycles (c).

Fig. 5 The initiation and development of plastic deformation in the first loading and unloading cycle. The plastic deformation initiated and developed when the indenter penetrated to the depth of 0.2 μm (a), 1 μm (b) and 2 μm (c), respectively. Fig.5 (d) indicates that the plastic deformation occurred during unloading process. At the displacement of approximately 0.9 μm, the indenter is fully separated from the surface. There is no visible

difference between (c) and (d), indicating no further plastic deformation occurred during unloading process.

Fig. 6 The plastic deformation developed through cyclic loading.

Fig. 7 The damage initiation and accumulation at the various depths of the coating over the loading cycles.

Fig. 8 The maximum principal stress distribution at the various penetration of the indenter over the loading cycles. Fig.8 a & b shows the maximum principal stress distribution during loading when the indenter is displaced at 2 μm and during unloading when the indenter is at 0.9 μm away from the reference point. Fig.8c shows that the first crack occurs at the 6th cycle during loading process when the indenter moves downward to the position of 1.5 μm from the reference point. Fig.8 d, e &f show that crack propagated through the thickness of coating into the 1μm in depth at 13th cycle, 1.4 μm at 103rd cycle, and remained at 1.4 μm until 273rd cycle.

Fig. 9 Crack performance during loading and unloading process; (Left) Crack performance during the loading after the crack is fully formed; (Right) Crack performance during unloading after the crack has formed.

fig.1

Click here to access/download;Figure;fig 1.pdf

Crack propagation of a thin hard coating under cyclic loading: Irreversible cohesive zone model

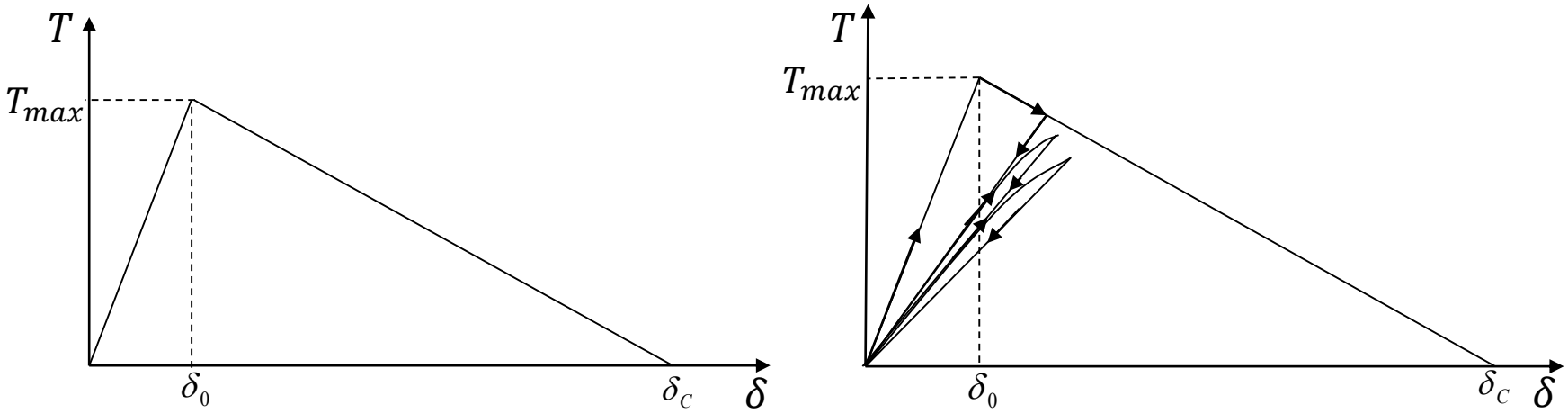

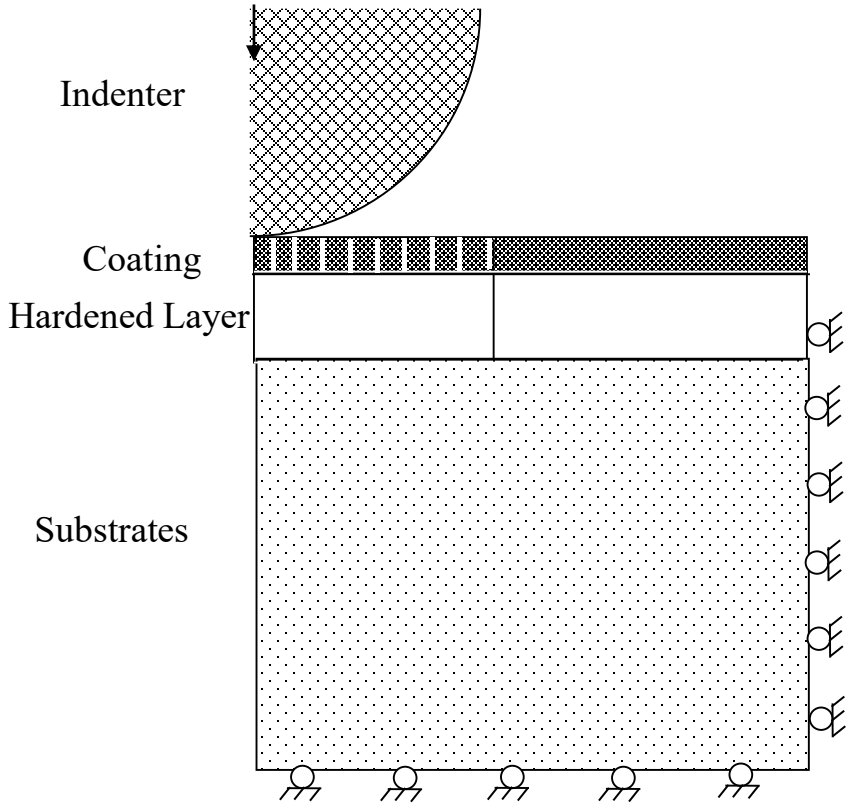

fig.3

Click here to access/download;Figure;fig 3.pdf

Crack propagation of a thin hard coating under cyclic loading: Irreversible cohesive zone model

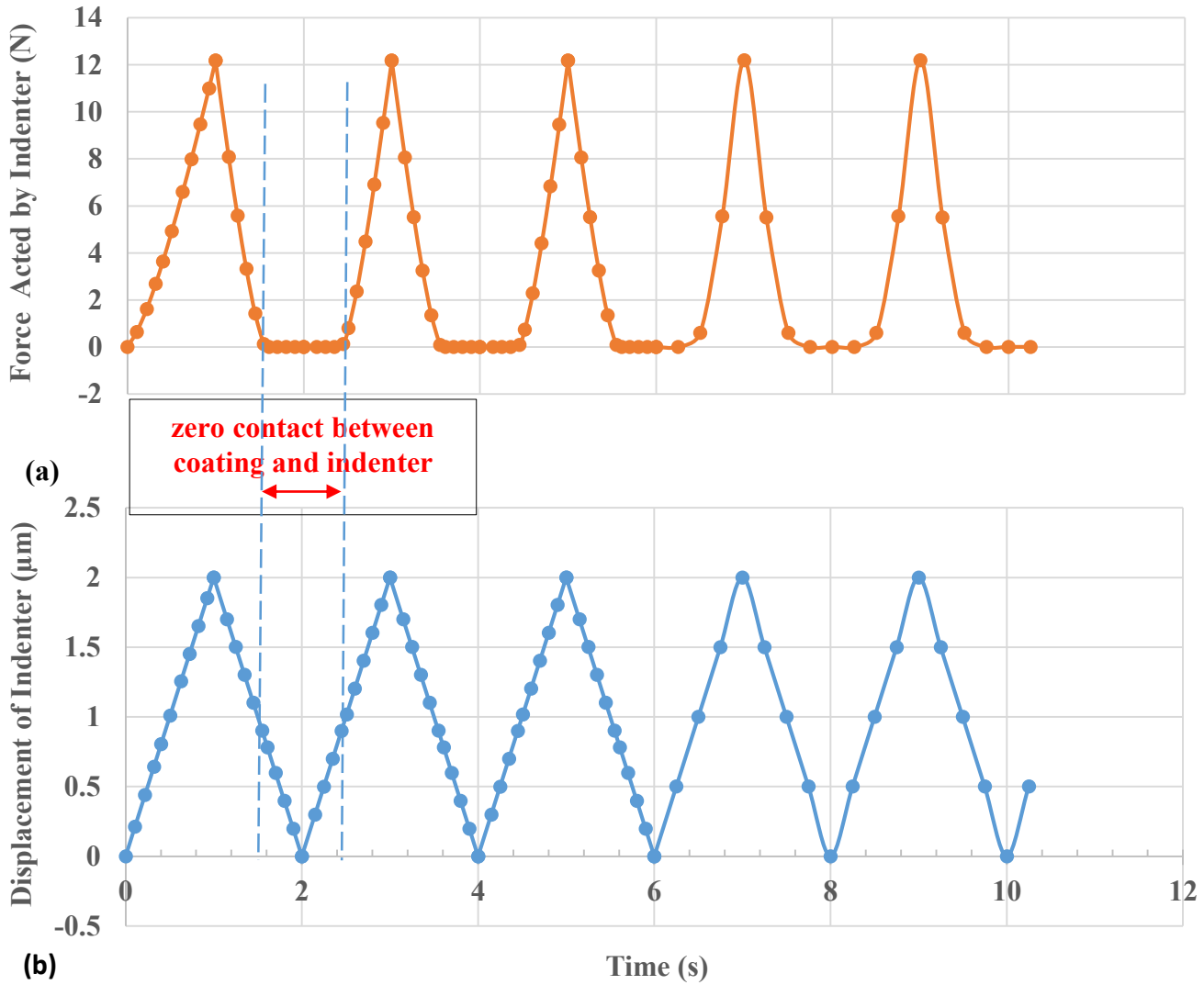

fig.4

Click here to access/download;Figure;fig 4.pdf

Crack propagation of a thin hard coating under cyclic loading: Irreversible cohesive zone model

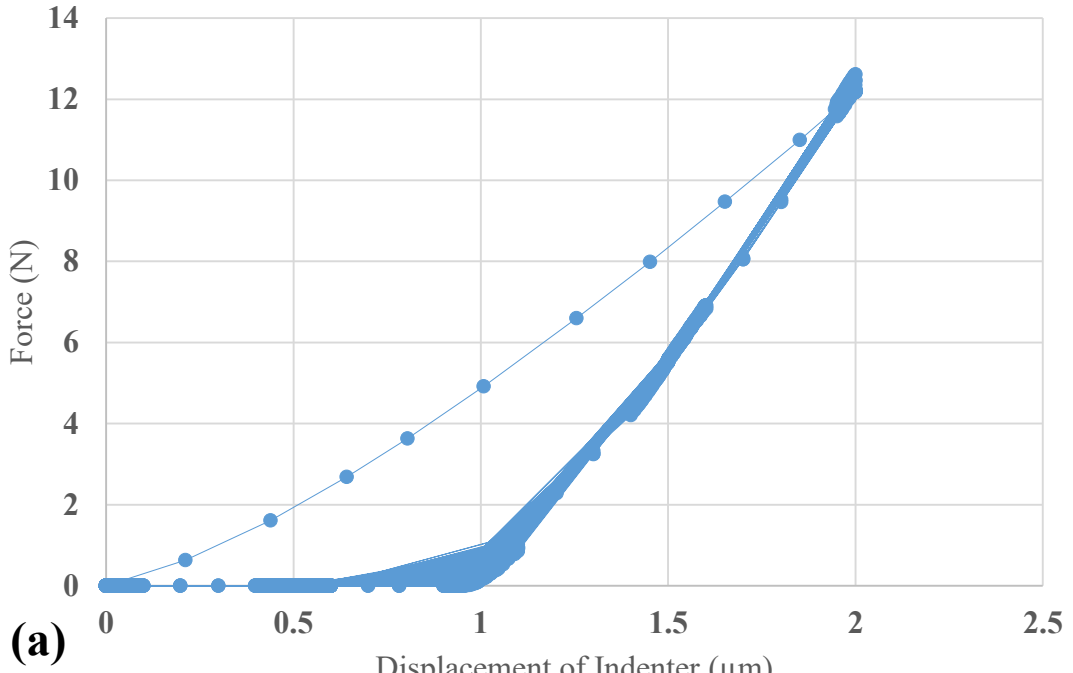

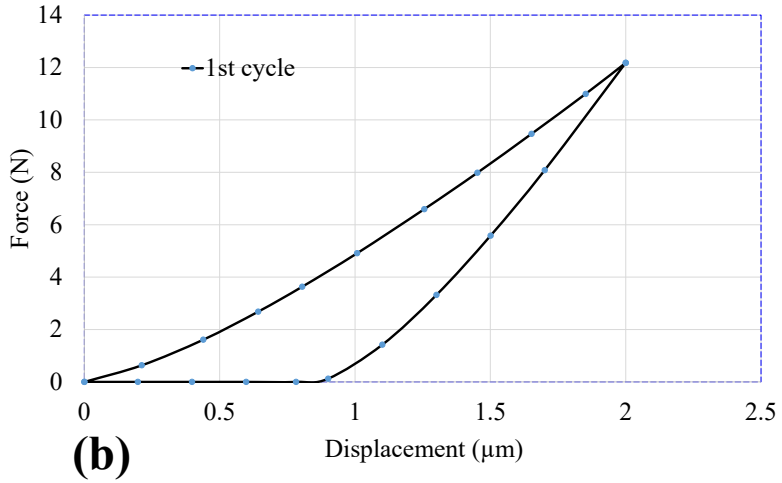

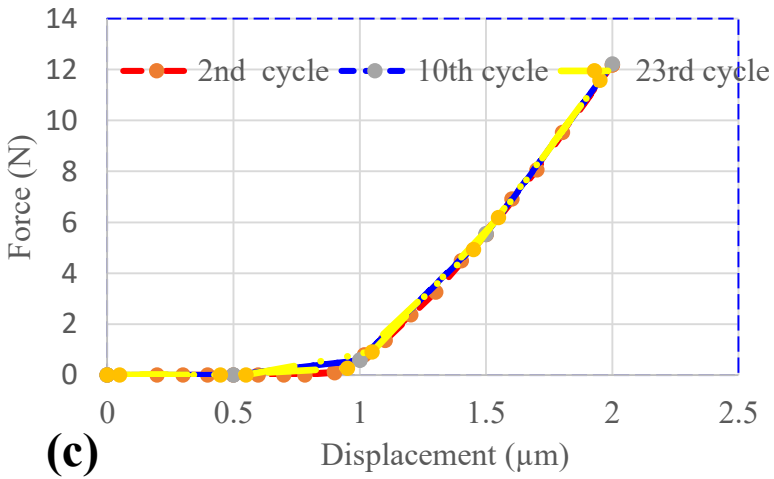

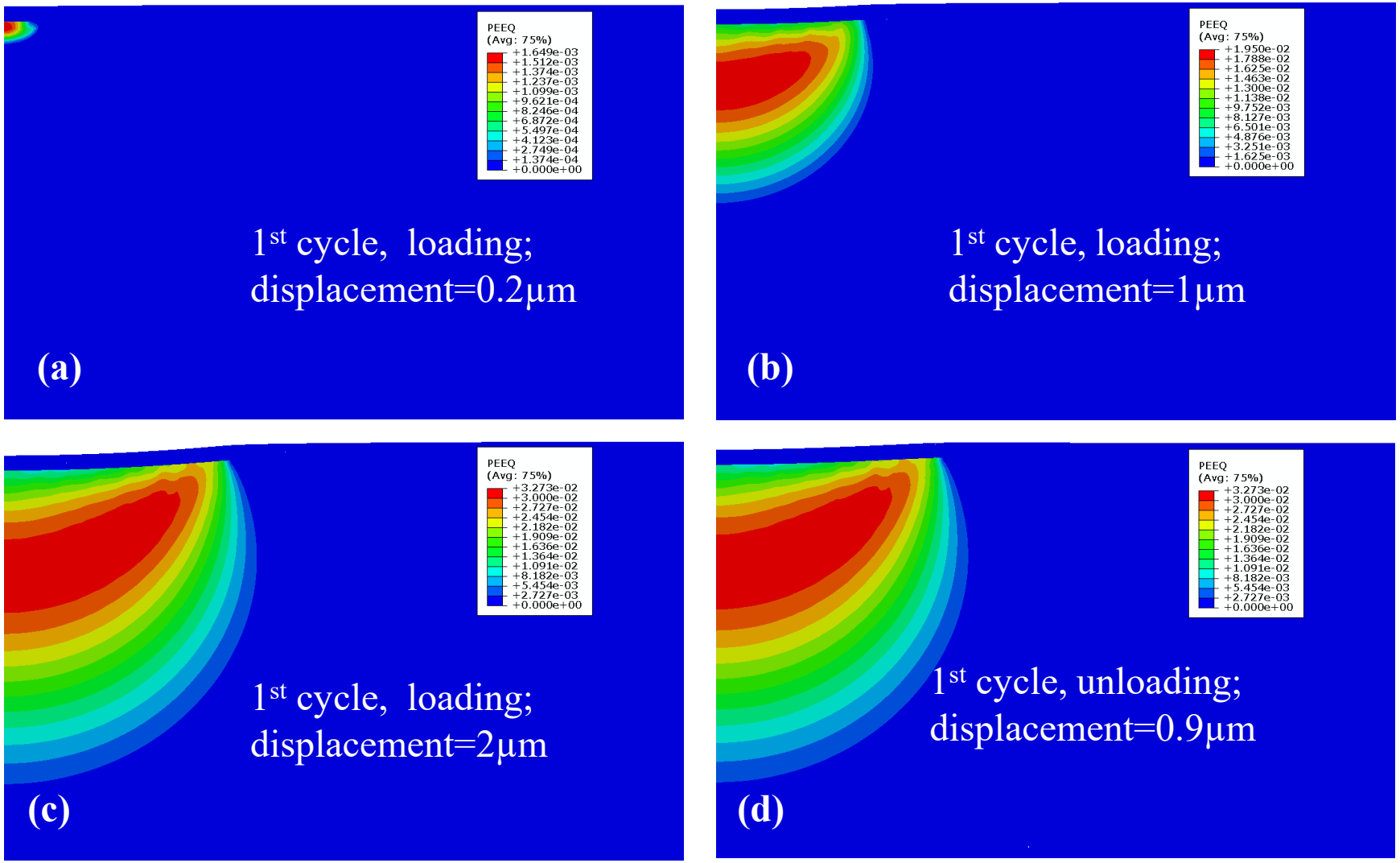

fig.6

Click here to access/download;Figure;fig 6.pdf

Crack propagation of a thin hard coating under cyclic loading: Irreversible cohesive zone model

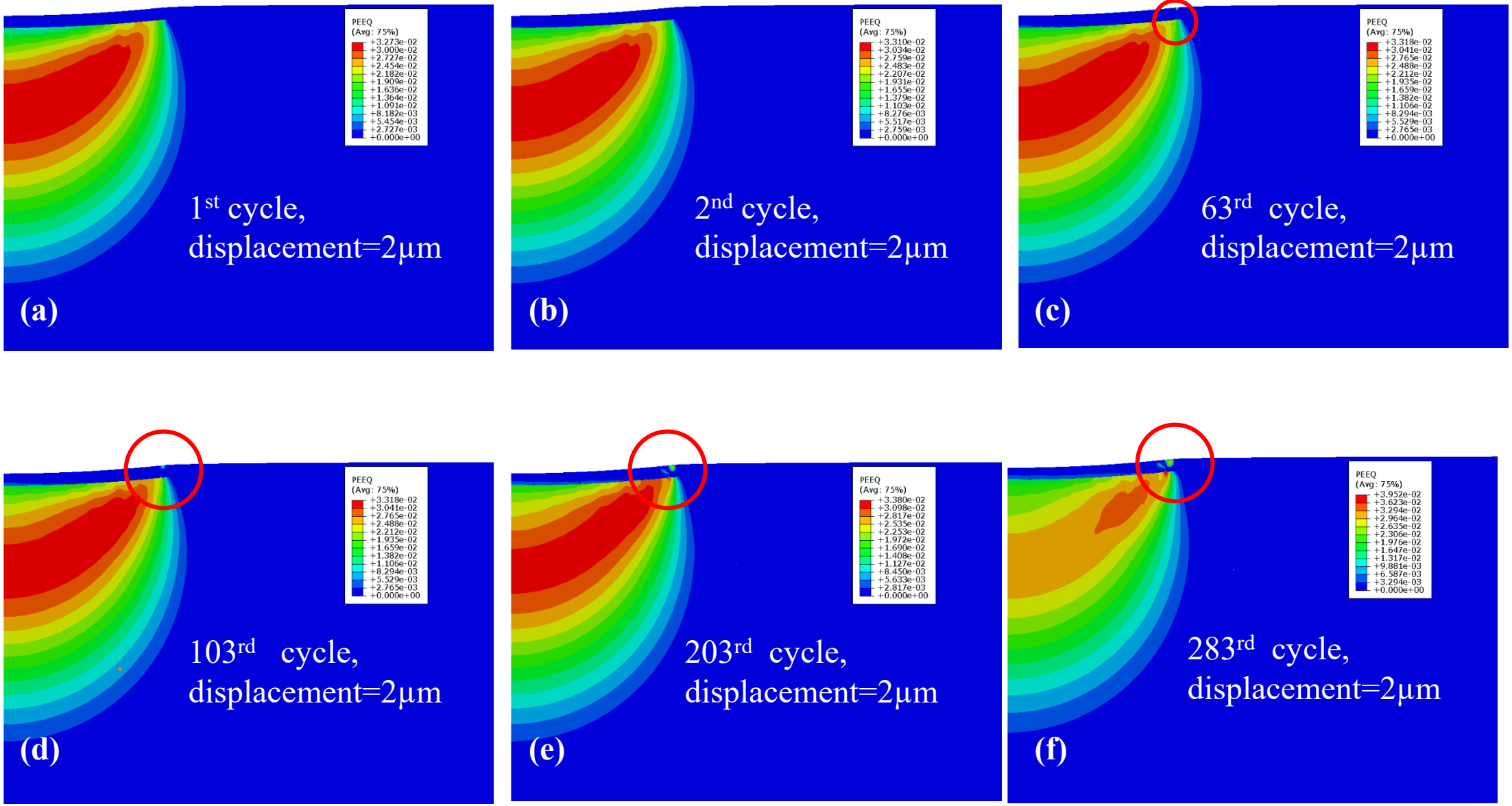

fig.7

Click here to access/download;Figure;fig 7.pdf

Crack propagation of a thin hard coating under cyclic loading: Irreversible cohesive zone model

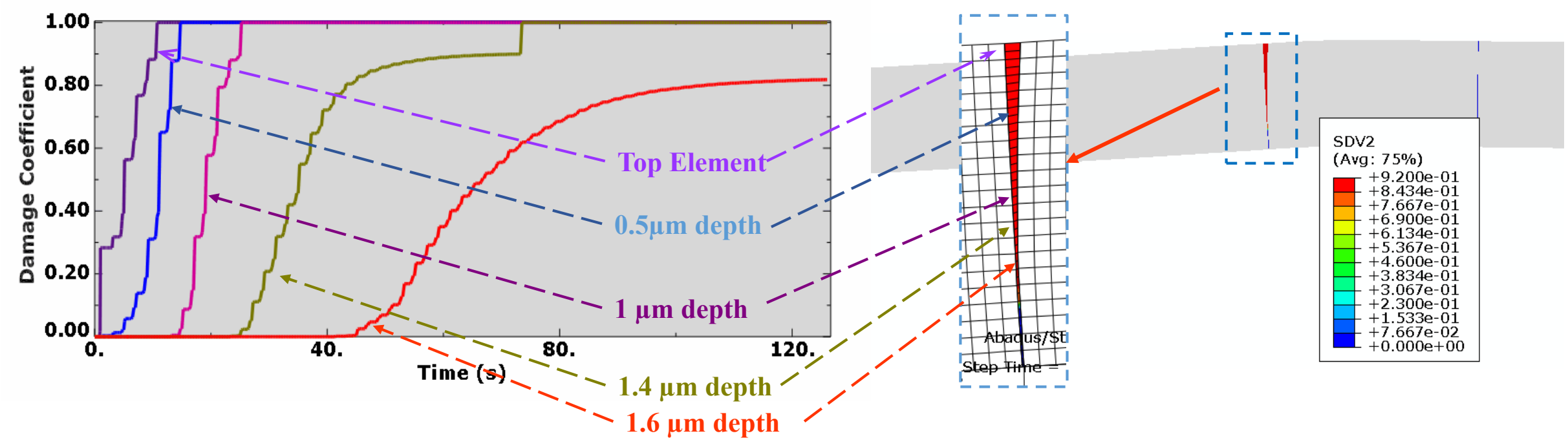

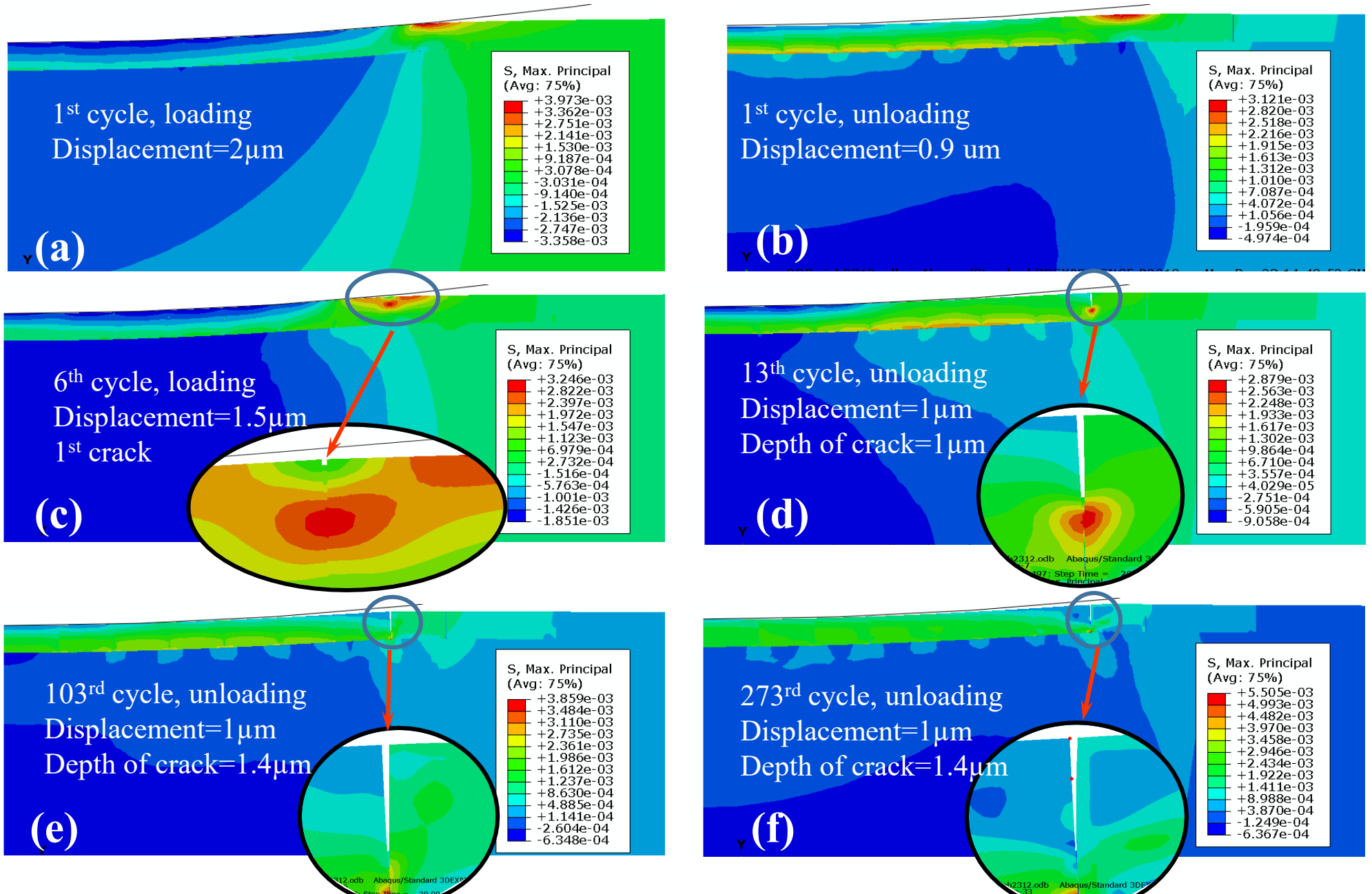

fig.9

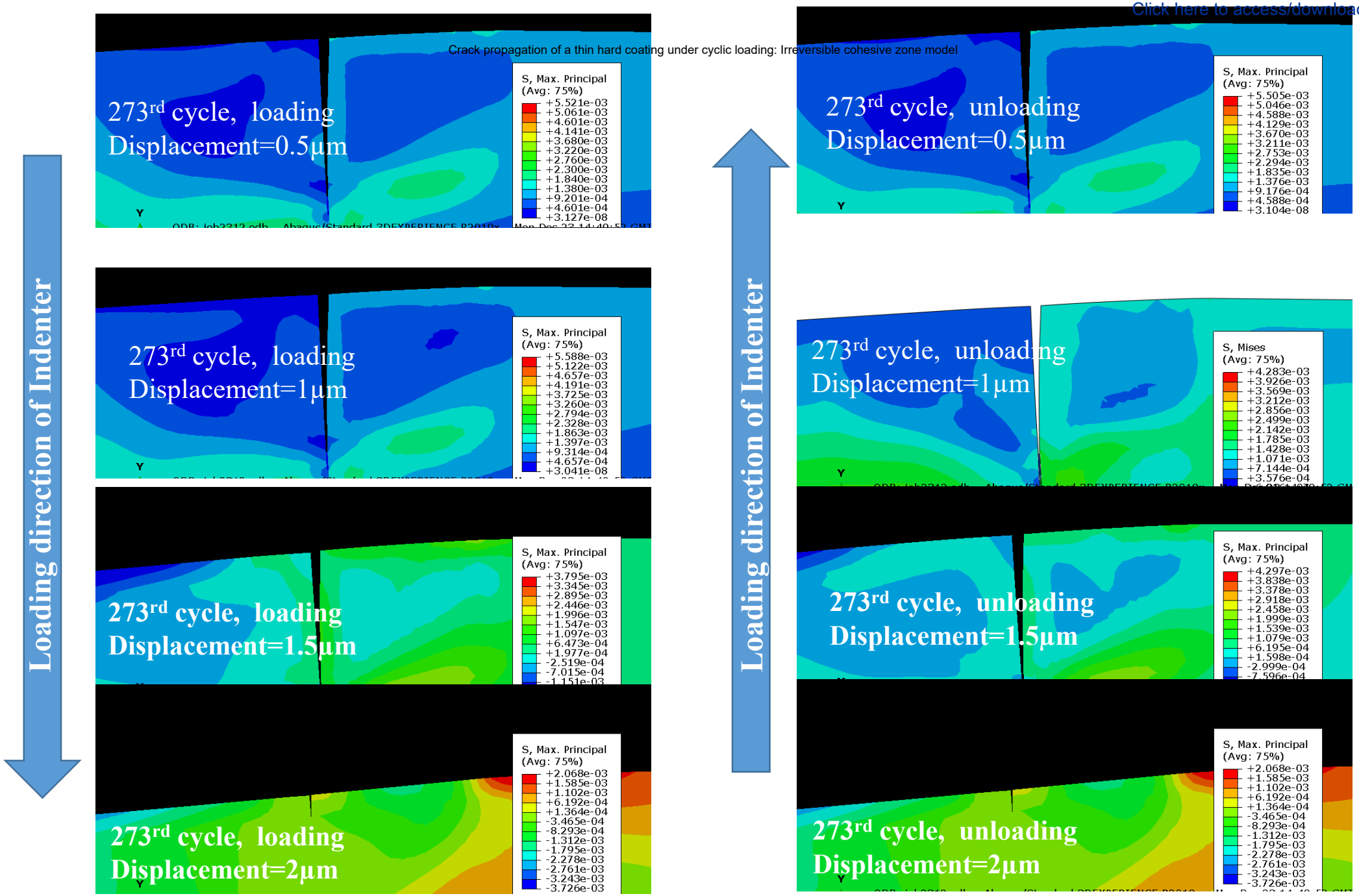

Graphical Abstract

Crack propagation of a thin hard coating under cyclic loading: Irreversible cohesive zone model

Plastic Deformation at the harden-case layer

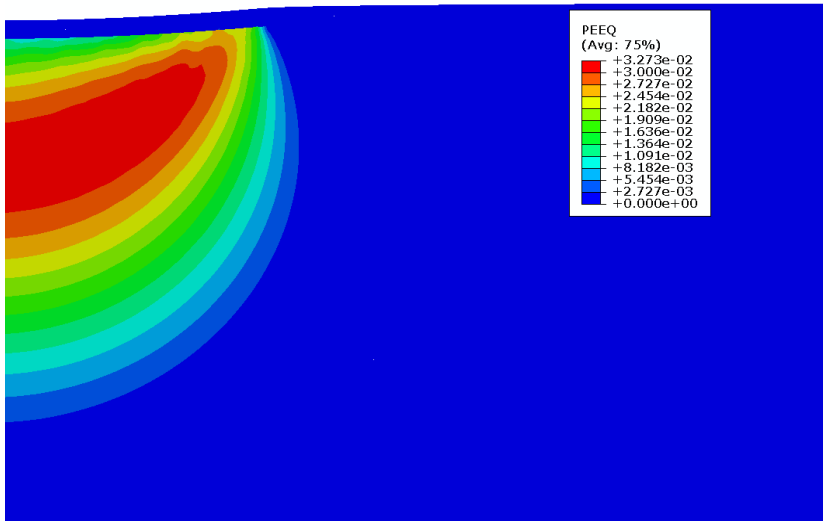

Maximum Principle Stress distribution during loading

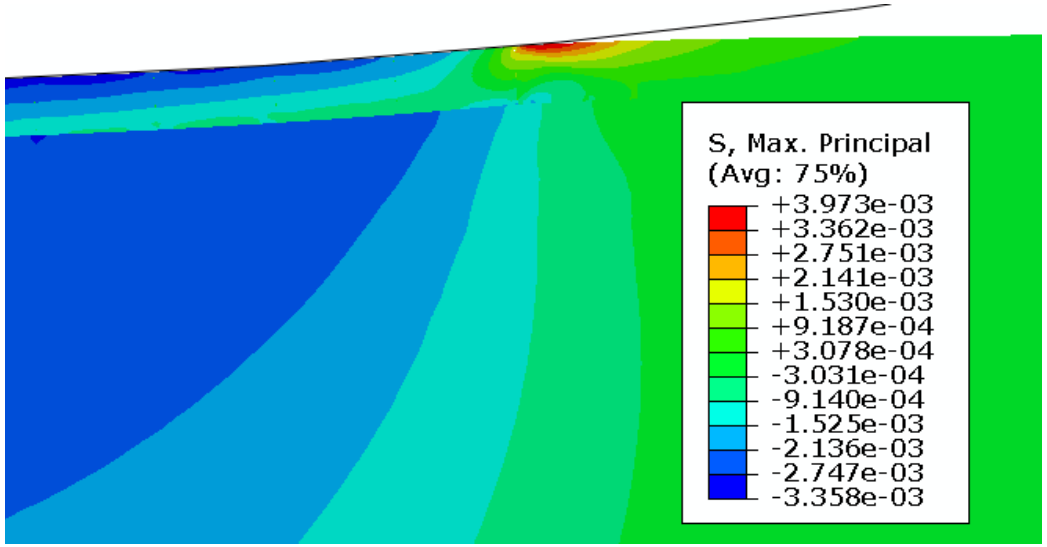

Damage coefficient developed with the loading cycles

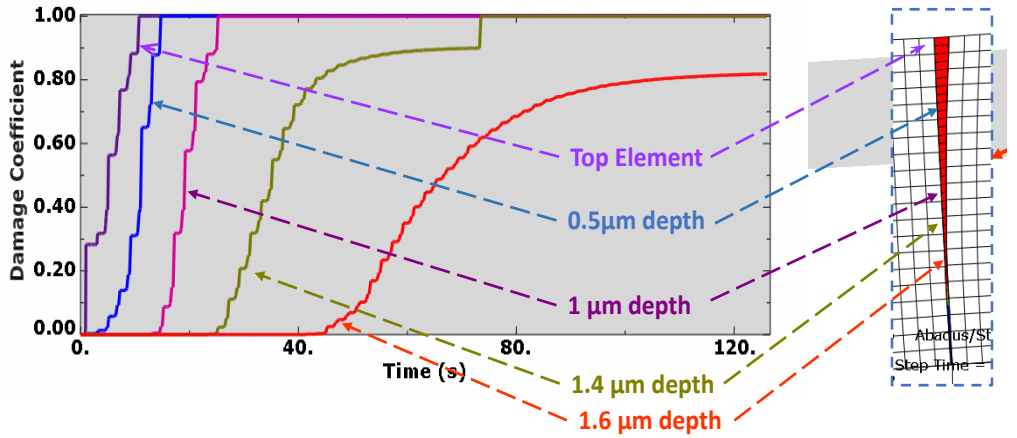

Crack initiation and propagation within the coating